A hybrid control framework for impulsive control of satellite rendezvous

Mirko Brentari, Denis Arzelier, Christophe Louembet, Sofia Urbina and Luca Zaccarian

Abstract— We focus on the problem of satellite rendezvous between two spacecraft in elliptic orbits. Using a linearized model of the relative dynamics, we first propose a periodic similarity transformation based on Floquet-Lyapunov theory, leading to a set of coordinates under which the free motion is linear time-invariant. Then we address the problem of impulsive control of satellite rendezvous as a hybrid dynamical system, and we show that the arising elegant representation enables designing impulsive control laws with different trade-offs between computational complexity and fuel consumption. The adopted hybrid formalism allows us to prove suitable stability properties of the proposed controllers. The results are comparatively illustrated on simulation examples.

I. INTRODUCTION

Considering the increasing need for satellite servicing in space, the capability of operating an active spacecraft, the *follower* denoted by F, in close proximity of a satellite, the *leader* denoted by L will be crucial for fulfilling complex safe space missions objectives comprising inspection, repairing, refueling or monitoring [6]. The whole relative spacecraft maneuvering process composes what is known as the rendezvous and proximity operations which mainly consists in getting the follower from one orbit to a box near the leader (close range rendezvous) [10], [5] and then in beginning the proximity operations required by the mission objectives. When dealing with the preliminary planning phase of space missions, it is usual to approximate actual finite-thrust powered phases of finite duration by impulsive maneuvers. The impulsive approximation for the thrust means that instantaneous velocity increments are applied to the chaser when firing, whereas its position is continuous. This assumption, made in this paper, has proved to be very useful in reducing the complexity of guidance and control design and has been widely used in the literature dedicated to rendezvous (see [6], [3], [5] and the references therein).

In this article, we are mainly interested by the first phase for which it is highly recommended to design fuel efficient impulsive maneuvers guiding the follower, from one point to a specified tolerance region in the proximity of the leader where the relative motion of the follower will be periodic and bounded. It is well known that, under Keplerian assumptions, the relative motion between spacecrafts is bounded [8]. Different conditions for the periodicity of the linearized

equations of the nonlinear relative motion have been given in the literature. For instance, the authors of [1] state that the identity of the semi-major axis of the spacecraft orbits is a necessary and sufficient condition for periodicity while Inalhan in [9] proposed a periodicity condition at perigee, for the linearized relative motion and for arbitrary eccentricity in a Cartesian and local framework. The well-known energy-matching condition, given by Gurfil in [8] involves a sixth degree polynomial equation. It is important to notice that different parametrizations (Cartesian coordinates, orbital elements) of the relative motion have been used in these previous developments. Recently, a new set of parametric expression for the relative motion has been given in the reference [3] and used to characterize in a very simple way periodic relative motions. In a linearized context, any relative periodic trajectory is defined by 6 constant parameters with the first one equal to 0.

Building on the result presented in [3], the contribution of the present paper is twofold. First, we propose a new coordinate transformation which leads to a simplified characterization of periodic trajectories when applied to the Tschauner-Hempel equations of the elliptic linearized relative motion. Second, three different hybrid feedback-control laws are designed by taking advantage of the particular formulation of the rendezvous problem. Indeed, in recent years, a novel framework has been proposed [7] for representing nonlinear hybrid dynamical systems whose solutions exhibit continuous evolution and impulsive behavior. In that context, suitable results about robust asymptotic stability of compact attractors have been proven. We adopt here that formalism, which allows us to state and prove suitable stability properties of the proposed impulsive control laws (including, e.g., the one originally presented in [5]) when applied to the linear time-varying dynamics of the closed-loop satellite rendezvous system.

Notations: e, ν and T are respectively the eccentricity, the true anomaly and the period of the leader's orbit. f' represents the derivation of the function f with respect to the true anomaly ν. Given a set $\mathcal{A} \subset \mathbb{R}^n$, $|x|_{\mathcal{A}} = \inf_{z \in \mathcal{A}} |x - z|$ denotes the distance of x from $\mathcal{A}$. I_n is the identity matrix of dimension n. For a set S, $\bar{S}$ denotes the closure of the set S.

II. LTI STATE-SPACE FOR THE LINEARISED RELATIVE EQUATIONS OF MOTION

The proximity operations between two spacecraft are characterized by the use of relative navigation since the separation between spacecraft is sufficiently small. In this framework, the relative motion of the follower is described in

the Local-Vertical-Local-Horizontal (LVLH) frame attached to the leader body [10]. The origin of the coordinate frame is located at the center of mass of the leader and the space is spanned by $(x,\ y,\ z)$ where z axis is in the radial direction (R-bar) oriented towards the center of the Earth, y axis is perpendicular to the leader orbital plane and pointing in the opposite direction of the angular momentum (H-bar) while x axis is chosen such that $x = y \times z$ (V-bar, see Figure 1).

Under Keplerian assumptions (no orbital perturbations are
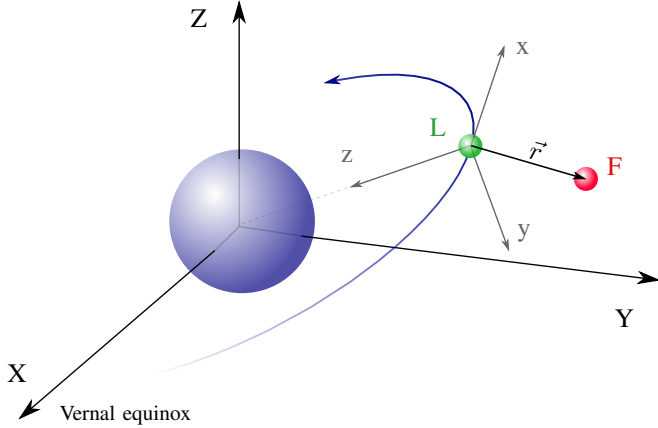

Fig. 1: Coordinates for relative spacecraft dynamics.

considered) and an elliptic reference orbit, the equation of motion for the relative motion in the LVLH frame may be linearized for close separation between the leader and the follower and are known as the Tschauner-Hempel (TH) equations [13], [12]:

$$\dot{\zeta} = A_0(t)\zeta \qquad\qquad \text{free motion}$$
$$\zeta^+ = \zeta + \begin{bmatrix} 0_{3\times3} \\ I_3 \end{bmatrix} \int_{t^-}^{t^+} \frac{f(t)}{m_F}\,dt \qquad \begin{array}{l}\text{when applying} \\ \text{impulsive thrusts,}\end{array} \quad (1)$$

where state $\zeta = (x, y, z, dx/dt, dy/dt, dz/dt)$ represents positions and velocities in the three fundamental axes of the LVLH frame, matrix A_0 is a suitable periodic function of time t [13], $f(t)$ is the thrust vector, ζ^+ is the state vector right after the jump and m_F is the mass of the follower. We may define the impulsive control input (essentially equivalent to velocity jumps in the three axes) as:

$$\Delta v(t_k) = \int_{t_k^-}^{t_k^+} \frac{1}{m_f} \begin{bmatrix} f_x(t) \\ f_y(t) \\ f_z(t) \end{bmatrix} dt, \qquad (2)$$

where t_k is a generic firing time, which is directly associated to the fuel consumption.

In order to simplify the TH equations, classical derivations correspond to applying a change of independent variable from time t to true anomaly ν, noting that:

$$\frac{d\nu}{dt} = \frac{n}{(1-e^2)^{3/2}} \underbrace{(1 + e\cos\nu)^2}_{\rho(\nu)} =: k^2\rho(\nu)^2, \qquad (3)$$

where $n = 2\pi/T$ is the mean motion of the leader orbit,

satisfying for any fixed ν_0, t_0:

$$\nu - \nu_0 = 2\pi \quad \Rightarrow \quad n(t - t_0) = 2\pi. \qquad (4)$$

This leads to the following hybrid representation for a new state $\xi(\nu)$, replacing $\zeta(t)$:

$$\xi' = A(\nu)\xi \qquad\qquad \text{free motion}$$
$$\xi^+ = \xi + \underbrace{\frac{1}{k^2\rho(\nu)^2} \begin{bmatrix} 0_{3\times3} \\ I_3 \end{bmatrix}}_{=:B(\nu)} u \qquad \begin{array}{l}\text{when applying} \\ \text{impulsive thrusts,}\end{array} \quad (5a)$$

where $u = \Delta v$ represents the applied impulse, state $\xi = (x, y, z, dx/d\nu, dy/d\nu, dz/d\nu)$ represents positions and velocities with respect to ν, and matrix A is given by (see [13], [12]):

$$A(\nu) = \begin{bmatrix} 0 & 0 & 0 & 1 & 0 & 0 \\ 0 & 0 & 0 & 0 & 1 & 0 \\ 0 & 0 & 0 & 0 & 0 & 1 \\ \frac{ec_\nu}{\rho} & 0 & -2\frac{es_\nu}{\rho} & 2\frac{es_\nu}{\rho} & 0 & 2 \\ 0 & -\frac{1}{\rho} & 0 & 0 & 2\frac{es_\nu}{\rho} & 0 \\ 2\frac{es_\nu}{\rho} & 0 & \frac{2+\rho}{\rho} & -2 & 0 & 2\frac{es_\nu}{\rho} \end{bmatrix}, \quad (5b)$$

where the dependence on ν has been omitted for brevity's sake and where we used $c_\nu = \cos(\nu)$ and $s_\nu = \sin(\nu)$.

Previous work [13], showed the usefulness of the following coordinate change for simplifying expression of dynamics (5):

$$T(\nu) = \begin{bmatrix} \rho(\nu)I_{3\times3} & 0_{3\times3} \\ \rho(\nu)'I_{3\times3} & \rho(\nu)I_{3\times3} \end{bmatrix}. \qquad (6)$$

In this article, we propose the two following additional transformations, the first one arising from similar observations to those in [5], and the second one arising from a suitable Floquet-Lyapunov derivation:

$$C(\nu) := \qquad\qquad\qquad\qquad\qquad\qquad\qquad\qquad (7)$$
$$\begin{bmatrix} 0 & c_\nu & 0 & 0 & -s_\nu & 0 \\ 0 & s_\nu & 0 & 0 & c_\nu & 0 \\ 1 & 0 & -\frac{3es_\nu(1+\rho)}{\rho(e^2-1)} & \frac{es_\nu(1+\rho)}{e^2-1} & 0 & \frac{\rho^2-ec_\nu-3}{e^2-1} \\ e & 0 & -3s_\nu & s_\nu(1+\rho) & 0 & c_\nu\rho \\ 0 & 0 & \frac{3(c_\nu+e)}{e^2-1} & -\frac{c_\nu(1+\rho)+e}{e^2-1} & 0 & s_\nu\rho \\ 0 & 0 & -\frac{3(3ec_\nu+e^2+2)}{e^2-1} & \frac{3\rho^2}{e^2-1} & 0 & -\frac{3es_\nu\rho}{e^2-1} \end{bmatrix}$$

$$S(\nu) := \begin{bmatrix} 1 & 0 & 0 & 0 & 0 & 0 \\ 0 & 1 & 0 & 0 & 0 & 0 \\ \hline 0 & 0 & 1 & 0 & 0 & \frac{\sigma(\nu)}{(1-e^2)^{3/2}} \\ 0 & 0 & 0 & 1 & 0 & 0 \\ 0 & 0 & 0 & 0 & 1 & 0 \\ 0 & 0 & 0 & 0 & 0 & 1 \end{bmatrix}, \qquad (8)$$

where we introduced the function:

$$\sigma(\nu) = (\nu - \tilde\nu) - n(t - \tilde t)$$
$$= (\nu - \tilde\nu) - (M - \tilde M)$$
$$= \Delta\nu - \Delta M, \qquad (9)$$

based on an arbitrary true anomaly value $\tilde\nu$ (in our simulations we select $\tilde\nu = 0$) corresponding to a specific time value

$\tilde{t}$ (in our simulations we select $\tilde{t}$). Function σ in (9) is clearly periodic and bounded, due to the geometric dependence of ν and M when the leader follows a Keplerian elliptic motion.

The following result establishes a first contribution of this paper showing that the dynamics (5) can be transformed to a convenient linear time-invariant form by exploiting transformations (6), (7), and (8). The proof of the lemma is omitted as it follows from straightforward (even though lengthy) mathematical derivations.

Lemma 1: Consider matrices in (6), (7), and (8). Then the following operation:

$$\widehat{\xi} = R(\nu)\xi := S(\nu)\,C(\nu)\,T(\nu)\xi\,, \tag{10}$$

is a linear time-varying coordinates change, namely $R(\nu)$ is invertible for all ν and R and R^{-1} are uniformly bounded. Moreover, R is periodic and transforms $A(\nu)$ into the following time-invariant form:

$$\widehat{A} = R'(\nu)R^{-1}(\nu) + R(\nu)A(\nu)R^{-1}(\nu)$$

$$= \begin{bmatrix} 0 & 0 & 0 & 0 & 0 & 0 \\ 0 & 0 & 0 & 0 & 0 & 0 \\ 0 & 0 & 0 & 0 & 0 & (1-e^2)^{-3/2} \\ 0 & 0 & 0 & 0 & 0 & 0 \\ 0 & 0 & 0 & 0 & 0 & 0 \\ 0 & 0 & 0 & 0 & 0 & 0 \end{bmatrix}. \tag{11}$$

From the peculiar structure (quasi Jordan form) of the dynamic matrix $\widehat{A}$, it is observed (as already emphasized for similar coordinate changes in [4], [5]), that any periodic free motion of the original dynamics (1) can be suitably parametrized by specific selections of the state $\widehat{\xi}$ with the last component being zero. It is therefore convenient representing the system in terms of the error with respect to a desired motion ξ^{ref}:

$$\xi^{ref} := [\xi_1^{ref}\ \xi_2^{ref}\ \xi_3^{ref}\ \xi_4^{ref}\ \xi_5^{ref}\ 0]^T, \tag{12}$$

so that one may analyze the dynamics of the mismatch $\tilde{\xi} = \widehat{\xi} - \xi^{ref}$ between the coordinate $\widehat{\xi}$ in (10) and a constant reference value in (12), representing a desired target periodic motion.

III. IMPULSIVE CONTROL OF THE RELATIVE DYNAMICS

The coordinate transformation presented in Lemma 1 of the previous section is a useful means for suitably designing an impulsive control law.

Assigning the firing times t_k in (2) and also the corresponding selections of $\Delta v(t_k)$. Among others one objective is to reduce as much as possible the fuel consumption well characterized in [11] when firing is achieved by 6 identical thrusters rigidly mounted to the satellite, and corresponding to the cost function $J = \sum_{t_k \in \mathcal{T}} |\Delta v_x(t_k)| + |\Delta v_y(t_k)| + |\Delta v_z(t_k)| = \sum_{t_k \in \mathcal{T}} |\Delta v(t_k)|_1$, where $\mathcal{T}$ is the set of the times when impulsive thrusts are applied and $|\cdot|_1$ denotes the 1-norm. A more convenient expression of J is given in terms of the representation in (2) and corresponds to:

$$J = \sum_{\nu_k \in \mathcal{V}} |u(\nu_k)|_1, \tag{14}$$

with $\mathcal{V}$ being the set of firing instants. Based on (14) we may formulate our control design problem as follows:

Problem 1: Given plant (1) and its equivalent form (5), design a state feedback impulsive control law selecting the firing instants ν_k, $k \in \mathbb{N}$ and the corresponding inputs $u(\nu_k)$ such that

(i) for any selection of reference (12), the point $\{\xi = \xi^{ref}\}$ is globally asymptotically stable for the closed loop dynamics;

(ii) the cost J is minimized over a family of possible input selections.

To solve Problem 1, in this section we will propose hybrid control laws relying on the presence of a timer τ in charge of the sequencing of the impulsive control actions. Then, using the hybrid systems notation in [7] and state $\tilde{\xi} = \widehat{\xi} - \xi^{ref}$, we may write the following general dynamic description of the closed loop, enjoying the desirable property that timers ν and τ evolve in the compact set $[0, 2\pi]$ and that the flow equation for $\tilde{\xi}$ is $\tilde{\xi}' = \widehat{A}\tilde{\xi}$, because $\widehat{A}\xi^{ref} = 0$:

$$\begin{cases} \tilde{\xi}' = \widehat{A}\tilde{\xi}, \\ \nu' = 1, \\ \tau' = -1, \end{cases} \quad (\tilde{\xi}, \nu, \tau) \in \mathcal{C}, \tag{15a}$$

$$\begin{cases} \tilde{\xi}^+ = \tilde{\xi}, \\ \nu^+ = 0, \\ \tau^+ = \tau, \end{cases} \quad (\tilde{\xi}, \nu, \tau) \in \mathcal{D}_\nu \tag{15b}$$

$$\begin{cases} \tilde{\xi}^+ = \tilde{\xi} + \widehat{B}(\nu)\gamma_u\left(\tilde{\xi}, \nu\right) \\ \nu^+ = \nu, \\ \tau^+ = \gamma_\tau\left(\tilde{\xi}, \nu\right), \end{cases} \quad (\tilde{\xi}, \nu, \tau) \in \mathcal{D}_u, \tag{15c}$$

In equation (15), the impulsive control law has been selected as a feedback controller:

$$u = \gamma_u(\tilde{\xi}, \nu). \tag{16}$$

Moreover, according to the coordinate change given in (10), and to the results of Lemma 1, matrix $\widehat{B}(\nu) = R(\nu)B(\nu)$, is a periodic function of ν arising from combining the similarity transformation in (10) with the input matrix in (5), and corresponds to the matrix reported in (13) at the top of next page.

Equation (15) is a compact representation of the impulsive feedback control action as a set of dynamical constraints that solutions should satisfy for their correct evolution. In particular, using an overall state $\eta = (\tilde{\xi}, \nu, \tau)$, this dynamics falls into the general class of systems studied in [7]:

$$\begin{aligned} \eta \in \mathcal{C}, & \quad \dot{\eta} = F(\eta), \\ \eta \in \mathcal{D}, & \quad \eta^+ \in G(\eta). \end{aligned} \tag{17}$$

In particular, for our model, the following selections are made:

$$\mathcal{D}_\nu := \mathbb{R}^6 \times \{2\pi\} \times [0, 2\pi], \tag{18a}$$

$$\mathcal{D}_u := \mathbb{R}^6 \times [0, 2\pi] \times \{0\}, \tag{18b}$$

$$\mathcal{D} := \mathcal{D}_\nu \cup \mathcal{D}_u, \tag{18c}$$

$$\mathcal{C} := \overline{(\mathbb{R}^6 \times [0, 2\pi] \times [0, 2\pi]) \setminus \mathcal{D}}, \tag{18d}$$

which, due to (18c), is a choice that prioritizes jumps. In

$$\widehat{B}(\nu) = \frac{1}{k^2\rho^2(1-e^2)} \begin{bmatrix} 0 & -(1-e^2)\rho s_\nu & 0 \\ 0 & (1-e^2)\rho c_\nu & 0 \\ -e(1+\rho)\rho s_\nu - \dfrac{3\sigma\rho^3}{(1-e^2)^{3/2}} & 0 & \dfrac{3\sigma e\rho^2 s_\nu}{(1-e^2)^{3/2}} - \rho^3 + \rho^2 - 2\rho \\ (1-e^2)(1+\rho)\rho s_\nu & 0 & (1-e^2)\rho^2 c_\nu \\ (1+\rho)\rho c_\nu + e\rho & 0 & -\rho^2 s_\nu \\ -3\rho^3 & 0 & 3e\rho^2 s_\nu \end{bmatrix} \quad (13)$$

particular, based on (15), functions F and G in (17) are selected as:

$$F(\eta) = \begin{bmatrix} \widehat{A}\tilde{\xi} \\ 1 \\ -1 \end{bmatrix}; \; G(\eta) = \bigcup_{i \in \{u,\nu\} \text{ s.t. } \eta \in \mathcal{D}_i} G_i(\eta) \quad (19a)$$

$$G_\nu(\eta) = \begin{bmatrix} \tilde{\xi} \\ 0 \\ \tau \end{bmatrix}; \; G_u(\eta) = \begin{bmatrix} \tilde{\xi} + \widehat{B}(\nu)\gamma_u\left(\tilde{\xi}, \nu\right) \\ \nu \\ \gamma_\tau\left(\tilde{\xi}, \nu\right) \end{bmatrix}. \quad (19b)$$

The proposed hybrid model (15), (18) (or its equivalent compact form in (17), (18), (19)), corresponds to the following intuitive behavior of our solutions.

- Timer ν is used as an additional state to keep track of the periodic time-varying nature of the dynamics. Using the jump set in (18a) ensures that the timer is reset to zero each time it reaches the value 2π, thereby being confined [1] to the compact set $[0, 2\pi]$;
- Thrusters are fired according to (15c) whenever $\eta \in \mathcal{D}_u$, namely when the timer τ crosses zero (see (18b)). Then, at each time during the evolution of the dynamics, state τ captures the information about how long we need to wait until the next impulsive control action.
- Each time an impulsive control action is triggered, the associated control law corresponds to the value of the two functions

$$\gamma_u : \mathbb{R}^6 \times [0, 2\pi] \to \mathbb{R}^3, \\ \gamma_\tau : \mathbb{R}^6 \times [0, 2\pi] \to [0, 2\pi], \quad (20)$$

the first one assigning the current selection of the impulsive input u (based on (16)), and the second one preassigning the time to wait until the next impulsive input should be applied. Note that the range of γ_τ is bounded so that solutions will only take values of τ in the bounded set $[0, 2\pi]$.
- Within the proposed hybrid context, the stability goal formulated in item (i) of Problem 1 is well characterized in terms of the stability properties of the bounded attractor:

$$\mathcal{A} := \{0\} \times [0, 2\pi] \times [0, 2\pi], \quad (21)$$

which may be analyzed using the tools of [7, Chapter 7], because selections (18), (19) satisfy the hybrid basic conditions of [7, Assumption 6.5].

IV. CONTROL LAWS

In this section, we propose three different selections for the impulsive control law (20) solving Problem 1. These selections are different in terms of performances trade-offs and are comparatively illustrated on the example studies of Section V.

A. Periodic norm-minimizing control

While formulation (15), (20) is general enough to allow for aperiodic optimized sampling, the simplest possible selection of function γ_τ in (20) is given by periodic thrusters firing, corresponding to a certain period $\bar{\nu} \in [0, 2\pi]$ fixed a priori. This is equivalent to the following constant selection:

$$\gamma_\tau(\tilde{\xi}, \nu) = \bar{\nu}, \quad (22)$$

encoding the fact that each pair of consecutive jumps has a fixed angular distance of $\bar{\nu}$.

Regarding the selection of the stabilizer γ_u, to be evaluated periodically, we make here a conservative selection leading to the useful feature that after each impulse, the state $\tilde{\xi}_6 = \xi_6$ is driven to zero, so that in the absence of noise the spacecraft evolves through periodic (therefore bounded) motions. In particular, the following optimal selection is chosen:

$$u^\star = \arg\min_u |\tilde{\xi}^+|^2, \text{ subject to:} \\ \tilde{\xi}^+ = \tilde{\xi} + \widehat{B}(\nu)u, \quad \tilde{\xi}_6^+ = 0. \quad (23)$$

Due to the specific structure of matrix function $\widehat{B}$ in (13) at the top of the page, we may provide an explicit form of the minimizer in (23) after defining the following quantities:

$$\hat{b}_6(\nu) = \frac{1}{k^2} \begin{bmatrix} \frac{3\rho}{e^2-1} \\ 0 \\ \frac{3e\sin(\nu)}{1-e^2} \end{bmatrix}, \; \hat{B}_6^\perp(\nu) = \begin{bmatrix} e\sin(\nu) & 0 \\ 0 & 1 \\ \rho(\nu) & 0 \end{bmatrix}, \quad (24a)$$

which clearly satisfy $\hat{b}_6(\nu)^T \hat{B}_6^\perp(\nu) = 0$ because matrix $\hat{B}_6^\perp(\nu)$ generates the orthogonal complement of $\hat{b}_6(\nu)$.

With these definitions in place, we may write the explicit

expression of the proposed control law as:

$$\gamma_u(\tilde{\xi}, \nu) = u_6 - \hat{B}_6^{\perp}(\nu)(\hat{B}(\nu)\hat{B}_6^{\perp}(\nu))^{-L}(\tilde{\xi} + \hat{B}(\nu)u_6)$$

$$\text{with } u_6 = -\frac{\hat{b}_6(\nu)}{|\hat{b}_6(\nu)|^2}\tilde{\xi}_6, \tag{24b}$$

where $M^{-L} = (M^T M)^{-1} M^T$ denotes the left pseudo-inverse of matrix M. The effectiveness of selection (24b) is stated in the next proposition.

Proposition 1: For any value of ν, the inverses in function (24) always exist and selection (24) coincides with the minimizer in (23), namely $\gamma_u(\tilde{\xi}, \nu) = u^{\star}$.

Proof: The existence of the inverses easily follows from the fact that

$$\det\left((\hat{B}(\nu)\hat{B}_6^{\perp}(\nu))^T(\hat{B}(\nu)\hat{B}_6^{\perp}(\nu))\right)$$
$$= (1-e)^2 + 2e(1+\cos(\nu)) > 0$$
$$|\hat{b}_6(\nu)|^2 = \frac{9\rho^4(\rho^2 + e^2\sin(\nu)^2)}{(1-e^2)^2} > 0,$$

which clearly indicates that the left inverse in the first line of (24b) and u_6 in the second line of (24b) can be evaluated.

To show that (24) coincides with the minimizer in (23), first notice that constraint $\tilde{\xi}_6^+ = 0$ is automatically ensured by $\hat{b}_6(\nu)^T\hat{B}_6^{\perp}(\nu) = 0$, which implies $\tilde{\xi}_6^+ = \hat{b}_6^T(\nu)u_6 = 0$. Therefore, noting that $\hat{B}_6^{\perp}(\nu)$ is the orthogonal complement of $\hat{b}_6(\nu)$, all possible inputs guaranteeing that $\tilde{\xi}_6^+ = 0$ are parametrized by $v^{\star}$ in:

$$u = u_6 + \hat{B}_6^{\perp}(\nu)v^{\star}. \tag{25}$$

Therefore, the solution to (23) corresponds to (25) with $v^{\star}$ being the solution to the following unconstrained least squares problem:

$$v^{\star} = \arg\min_v |\tilde{\xi} + \hat{B}(\nu)u_6 + \hat{B}(\nu)\hat{B}_6^{\perp}(\nu)v|^2. \tag{26}$$

Then, as is well known (see, e.g., [2, Ex.1 pg 92]), the minimizer $v^{\star}$ is given by:

$$v^{\star} = -(\hat{B}(\nu)\hat{B}_6^{\perp}(\nu))^{-L}(\tilde{\xi} + \hat{B}(\nu)u_6),$$

which, substituted in (25), gives (24b), as to be proven. ∎

Remark 1: Based on Proposition 1, a desirable property of control law (22) (24) is that it instantaneously minimizes the norm of $\tilde{\xi}$ constrained to the fact that the subsequent motion be periodic. Since the norm of $\hat{b}_6$ in (24a) is never zero, then clearly, equation (24b) is always well-posed and ensures that $\tilde{\xi}_6^+ = 0$. In addition to this, instantaneously minimizing the norm of $\tilde{\xi}$ also ensures the best possible decrease at the specific fixed instant of time enforced by the rigid periodic selection. With this logic in place, we can guarantee stability of the closed-loop but not convergence. Indeed, we can guarantee non-increase of $|\tilde{\xi}|$ across jumps but there is no guarantee of obtaining a strict decrease. As a result, we anticipate a slow convergence (if any) in our simulation section when using this controller. Despite this fact, the choice (22) (24) is still an interesting one because it ensures that approaching between the two satellites is performed through periodic (bounded) motions, leading to some degree of fault tolerance (in case of malfunctioning,

the satellite is on a stable orbit). ○

The following theorem certifies that the proposed controller solves part of item (i) of Problem 1.

Theorem 1: Given control law (22) (24), the attractor $\mathcal{A}$ is uniformly globally stable along the arising closed-loop dynamics with (15).

Proof: First notice that $|(\tilde{\xi}, \nu, \tau)|_{\mathcal{A}} = |\tilde{\xi}|$. Recall that solutions $(\mu, j) \mapsto \tilde{\xi}(\mu, j)$ to hybrid systems have a domain $\text{dom}\,\tilde{\xi}$ parametrized by a flowing direction (here represented by the amount μ of true anomaly elapsed since the initial condition, as opposed to continuous time t for a classical hybrid systems representation) and by a jumping direction j (see [7, Chap. 2] for details). We first realize that before the first impulse, all solutions evolve in free motion along the LTI flow dynamics in (15), leading to:

$$|\tilde{\xi}(\mu, 0)| \leq |\exp(2\pi\hat{A})||\tilde{\xi}(0,0)|. \tag{27}$$

Notice now that Proposition 1 ensures that $\gamma_u(\tilde{\xi}, \nu) = u^{\star}$. In particular, after the first jump the state $\tilde{\xi}_6$ remains at zero for all (hybrid) times. Then during all subsequent flows, the state $\tilde{\xi}$ remains constant due to the structure of $\hat{A}$. Moreover, across jumps, the control law is the minimizer of (23), clearly satisfying $|\tilde{\xi}^+| \leq |\tilde{\xi}|$. As a consequence, we get

$$|\tilde{\xi}(\mu, j)| \leq |\exp(2\pi\hat{A})||\tilde{\xi}(0,0)|, \tag{28}$$

for all $(\mu, j) \in \text{dom}\,\tilde{\xi}$, which establishes uniform global stability. ∎

B. Periodic bi-impulsive control

A second selection that we propose for the controller in (20) is once again periodic, thereby corresponding to selection (22) for γ_τ. However, it corresponds to a wiser selection of γ_u (in terms of envisioned fuel consumption), performed in similar ways to what is proposed in [5], by focusing on the overall effect on the state $\tilde{\xi}$ of two impulses performed at a distance of $\bar{\nu}$ from one another. In particular, using straightforward computations, if two impulses u_1 and u_2 happen at times μ_1 and $\mu_2 = \mu_1 + \bar{\nu}$, we obtain, along the corresponding solution:

$$\Phi(-\bar{\nu})\tilde{\xi}(\mu_2, j+2) = \tilde{\xi}(\mu_1, j)$$
$$+ \underbrace{\left[\hat{B}(\nu_1) \quad \Phi(-\bar{\nu})\hat{B}(\nu_1 + \bar{\nu})\right]}_{M(\nu_1, \bar{\nu}) :=}\begin{bmatrix} u_1 \\ u_2 \end{bmatrix} \tag{29}$$

where μ_1, μ_2 denote the (angular) times, j denotes the number of elapsed thruster firings, $\Phi(\mu) = e^{\hat{A}\mu} =$
$$\begin{bmatrix} 1 & 0 & 0 & 0 & 0 \\ 0 & 1 & 0 & 0 & 0 \\ 0 & 0 & 1 & 0 & \mu(1-e^2)^{-3/2} \\ 0 & 0 & 0 & 1 & 0 \\ 0 & 0 & 0 & 0 & 1 \end{bmatrix}$$ is the state transition matrix of the
(LTI) flow dynamics in (15), and $\nu_1 = \nu(\mu_1, j)$.

Based on relation (29), and to the end of selecting u_1, u_2 in such a way that $\tilde{\xi}(\mu_2, j+2)$ is zero, it is important to study the invertibility properties of matrix $M(\nu, \bar{\nu})$, which is done in the following conjecture. The result of the conjecture restricts the set of possible selections of $\bar{\nu}$ in (22).

Conjecture 1: For any value of $\nu \in [0, 2\pi]$, matrix $M(\nu, \bar{\nu})$ in (29) is invertible if and only if $\bar{\nu} \neq k\pi$, $k \in \mathbb{Z}$.
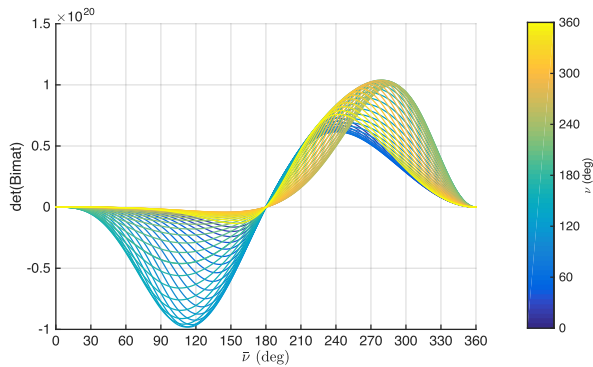
Fig. 2: Determinant of matrix $M(\nu, \bar{\nu})$ with $e = 0.4$.

Conjecture 1 is motivated by numerical experience and its formal proof is regarded as future work. In support of the conjecture, we report in Figure 2 the value of the determinant of $M(\nu, \bar{\nu})$ for different values of ν (represented by the color code) and $\bar{\nu}$ (represented by the horizontal axis). The plot corresponds to the value $e = 0.4$. If Conjecture 1 holds, for any selection $\bar{\nu} \in (0, 2\pi) \setminus \{\pi\}$, equation (29) can be inverted to compute the unique pair of inputs $u_1^\star, u_2^\star$ ensuring $\tilde{\xi}(\mu_2, j + 2) = 0$ (namely that the state $\tilde{\xi}$ is driven to zero after two impulses separated by $\bar{\nu}$ times). Then, following a receding horizon type of paradigm, we may apply the first pulse and re-evaluate the control law at the next pulse. The above control design paradigm leads to the following selection:

$$\gamma_u(\tilde{\xi}, \nu) = -\begin{bmatrix} I & 0 \end{bmatrix} M(\nu, \bar{\nu})^{-1} \tilde{\xi}. \tag{30}$$

Then, the overall control strategy (22), (30) guarantees item (i) of Problem 1 as established in the next theorem.

Theorem 2: Given $\bar{\nu} \in (0, 2\pi) \setminus \{\pi\}$, assume that matrix $M(\nu, \bar{\nu})$ is invertible for any value of $\nu \in [0, \pi]$.

Then, control law (22), (30) ensures that attractor $\mathcal{A}$ in (21) is uniformly globally asymptotically stable along the arising closed-loop dynamics with (15).

Proof: The proof is carried out by exploiting the following global version of [7, Prop. 7.5] (its proof is straightforward, taking $\mu \to \infty$ in the semiglobal version of [7, Prop. 7.5], and is actually therein implicitly used for establishing the result in [7, Ex. 7.6]).

Proposition 2: Given a nominally well-posed hybrid system $\mathcal{H}$, suppose that the compact set $\mathcal{A}$ in (21) is strongly forward invariant and globally uniformly attractive for $\mathcal{H}$. Then, it is uniformly globally asymptotically stable for $\mathcal{H}$.

To apply Proposition 2 in our case, we first notice that the data of hybrid system (15), (22), (30) satisfies the hybrid basic conditions in [7, As. 6.5], therefore, from [7, Thm 6.8], it is nominally well-posed. Concerning forward invariance of $\mathcal{A}$ (namely, all solutions starting in $\mathcal{A}$ remain in $\mathcal{A}$ for all times), it follows from the fact that the flow dynamics of $\tilde{\xi}$ is linear (so the origin is an equilibrium) and the jumps guarantee non-increase of $\tilde{\xi}$ (see the proof of Theorem 1). Finally, global uniform convergence is a straightforward consequence

of a stronger property of uniform finite-time convergence enjoyed by closed-loop (15), (22), (30). In particular, all solutions converge in finite time to $\mathcal{A}$ after two impulses. Indeed, consider two subsequent impulses associated to the control selections $u_j = \begin{bmatrix} I & 0 \end{bmatrix} \begin{bmatrix} u_{j,1} \\ u_{j,2} \end{bmatrix} = u_{j,1}$ and $u_{j+1} = \begin{bmatrix} I & 0 \end{bmatrix} \begin{bmatrix} u_{j+1,1} \\ u_{j+1,2} \end{bmatrix} = u_{j+1,1}$. Then, due to the property that $\begin{bmatrix} u_{j,1} \\ u_{j,2} \end{bmatrix}$ brings the state to zero after two impulses, it follows that selection $\begin{bmatrix} u_{j+1,1} \\ u_{j+1,2} \end{bmatrix} = \begin{bmatrix} u_{j,2} \\ 0 \end{bmatrix}$ is a feasible one for the second impulse. As a consequence of uniqueness, arising from relation (29), this is the only possible solution and we must have $\tilde{\xi}^+ = 0$ after the second impulse, which implies uniform finite-time convergence to $\mathcal{A}$, as to be proven. ∎

C. Non-periodic bi-impulsive control

With the goal of minimizing the fuel consumption, a main drawback of the strategies proposed in the two previous sections is the fact that the (angular) time elapsed between two consecutive impulses is fixed and equal to $\bar{\nu}$. This is indeed a direct consequence of the simplified selection (22). In this section, we propose a different control paradigm, corresponding to an increased computational complexity, where the bi-impulsive control paradigm in (30) is combined with an optimized selection of the waiting time τ^+ before the next impulse. In particular, the overall control law corresponds to:

$$\gamma_\tau(\tilde{\xi}, \nu) = \arg\min_{\bar{\nu} \in [0, 2\pi]} \left| M(\nu, \bar{\nu})^{-1} \tilde{\xi} \right|_1 = \arg\min_{\bar{\nu} \in [0, 2\pi]} J, \tag{31a}$$

$$\gamma_u(\tilde{\xi}, \nu) = -\begin{bmatrix} I & 0 \end{bmatrix} M(\nu, \gamma_\tau(\tilde{\xi}, \nu))^{-1} \tilde{\xi}. \tag{31b}$$

The new control law (31) corresponds to selecting an optimal elapsed time μ before the next impulse, according to the fuel consumption index (14). In particular, the corresponding optimization is nonlinear and, because of Conjecture 1, corresponds to minimizing the argument in the two intervals $(0, \pi)$ and $(\pi, 2\pi)$ where matrix $M(\nu, \cdot)$ is invertible. Then, the minimum can be selected as the minimum of the two minimizers. For illustration purposes, Figure 3 shows the values of $M(\nu, \bar{\nu})$ for the three first initial conditions considered in the simulations of Section V. Notice that in the first two cases the functions are rather similar. Instead, the third case (lower plot of Figure 3) corresponds to a significantly different function where the global minimum is obtained in the first interval.

As compared to the previous controllers, control law (31) is associated with an increased computational complexity. Indeed, at each impulse time a numerical optimization providing the solution to (31a) needs to be performed. Nonetheless, the advantages in terms of fuel consumption are clearly illustrated by the simulation results of the next section. It should be emphasized that the minimization is carried out over a compact set $[0, 2\pi]$, so it may be easily performed following some heuristics. Numerical evidence reveals that the functions in Figure 3 are strictly convex in the intervals $(0, \pi)$ and $(\pi, 2\pi)$. Formally proving this property (which is subject of future work) may allow for very efficient convex optimization methods to evaluate control law (31).
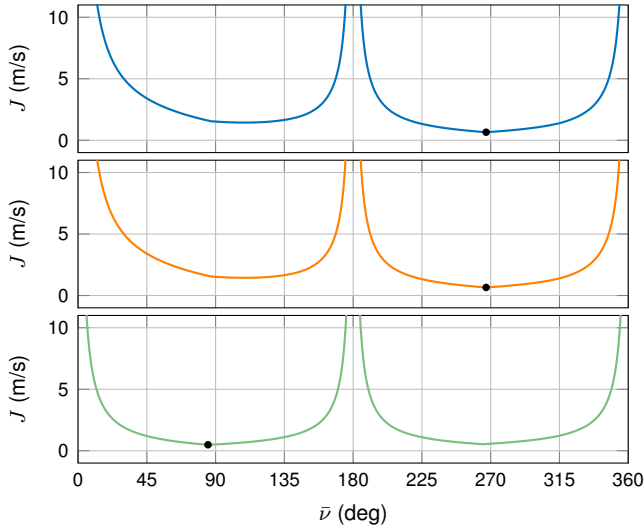
Fig. 3: Value of the function at the right hand side of (31a) for the three first initial conditions considered in Section V.

The following result can be established by similar derivations to those in the proof of Theorem 2, relying on the uniqueness of the solution to the inverse of equation (29). This, together with the optimal selection of γ_τ in (31) provides a solution to both items (i) and (ii) of Problem 1.

Its proof is omitted due to this similarity to that of Theorem 2.

Theorem 3: Control law (31) ensures that attractor $\mathcal{A}$ in (21) is uniformly globally asymptotically stable along the arising closed-loop dynamics with (15).

V. SIMULATIONS

In this section, we present the simulation results obtained with the control laws designed in Section IV and system (15) (equivalently (17)–(19)) using a linearized model simulator. In these simulations, an orbit with a semi-major axis of 7011 km and eccentricity of 0.4 will be considered for the leader vehicle. The simulations aim at stabilizing a periodic trajectory specified by a suitable selection of ξ^{ref} in (12), which is free to evolve inside a tolerance box $\mathcal{B}$. The tolerance box $\mathcal{B}$ is centered at the target's position coordinate ζ_f (expressed in the frame used in (1)) and has positive and negative widths ζ_{tol} in the three LVLH directions, where:

$$\zeta_f = [100\ 0\ 0]^T \text{ m}$$
$$\zeta_{tol} = [150\ 25\ 25]^T \text{ m}.$$

In [3], a method is introduced to obtain the value of ξ^{ref} in (12) ensuring that the corresponding periodic evolution in the LVLH coordinates is always contained in the tolerance box $\mathcal{B}$. The resulting values of the reference state ξ^{ref} correspond to:

$$\xi^{ref} = [15.18\ \ 17.68\ \ 97.98\ \ 22.49\ \ -17.63\ \ 0]^T,$$
(32)

where we emphasize that the last element is zero (a necessary and sufficient condition for periodic motion).

For each one of the three control laws in Section IV, four different initial conditions ζ_0 for state ζ in (1) have been used, selected as:

$$\zeta_{01} = [500\ \ 400\ \ 10\ \ 0\ \ 0\ \ 0]^T,$$
$$\zeta_{02} = [-200\ \ 100\ \ 200\ \ 0\ \ 0\ \ 0]^T,$$
$$\zeta_{03} = [100\ \ -350\ \ -20\ \ 0\ \ 0\ \ 0]^T,$$
$$\zeta_{04} = [320\ \ 0\ \ -64\ \ 0\ \ 0\ \ 0]^T,$$
(33)

where in (33) the first three components are meters and the last three are meters per second. The initial relative velocity has been selected to be zero to account for the fact that the starting point of our trajectory may be a holding point arising from a previous station keeping along the space mission. Note that ζ_{04} is chosen to lie in the orbital plane of the target (the second component is zero).

The four initial conditions ζ_{01}, ζ_{02}, ζ_{03} and ζ_{04} in (33) correspond to four different initial distances from the tolerance box $\mathcal{B}$:

$$|\zeta_{01}|_{\mathcal{B}} = 512.9571 \text{ m} \tag{34a}$$
$$|\zeta_{02}|_{\mathcal{B}} = 314.2451 \text{ m} \tag{34b}$$
$$|\zeta_{03}|_{\mathcal{B}} = 325.0000 \text{ m} \tag{34c}$$
$$|\zeta_{04}|_{\mathcal{B}} = 326.3372 \text{ m} \tag{34d}$$

with the distance from the bounding box $\mathcal{B}$ being defined as:

$$|\zeta|_{\mathcal{B}} = |dz_{\zeta_{tol}}(\zeta_{1..3} - \zeta_f)|, \tag{35}$$

where $\zeta_{1..3} = (x, y, z)$ contains the first three components of state ζ in (1) and $dz_{\zeta_{tol}}(x)$ is the decentralized vector dead-zone function with limits ζ_{tol}.

The initial leader true anomaly values ν_0 vary from 0 to 360 degrees in equally spaced intervals of 10 degrees. All our simulations have been performed from the initial true anomaly ν_0 up to a final true anomaly $\nu_f = \nu_0 + 20\pi$, namely ten orbital periods later.

Two performance indexes are considered: the fuel consumption J in (14) and the true anomaly ν_B or angular time in terms of orbital periods (time elapsed when whe follower first reaches the bounding box $\mathcal{B}$). Figures 4 and 5 represent respectively these two indexes fixing each one of the initial conditions in (33) and using the three control laws in Section IV, where:

- the orange line ($-\times-$) refers to controller (22), (24) of Section IV-A, with the selection $\bar{\nu} = \pi/2$ in (22);
- the blue line ($-\circ-$) refers to controller (22), (30) of Section IV-B, with the same firing interval $\bar{\nu} = \pi/2$;
- the green line ($-\triangleleft-$) refers to the response using controller (31) discussed in Section IV-C, where the firing interval is optimized by the controller in order to reduce the fuel consumption J.

Figure 4 shows the cost J for each control law when the leader's initial true anomaly ν_0 varies. From this figure it is possible so see that for every initial state ζ_0 and every control law, the minimum cost always appears in the proximities of 180 (deg), corresponding to the apogee of the orbit.

It would be interesting therefore to perform the satellite maneuver when the leader's initial true anomaly ν_0 lies in the neighborhood of this value in order to minimize the amount of dispensed fuel. As expected, controller (31) always leads to the minimum value of J.
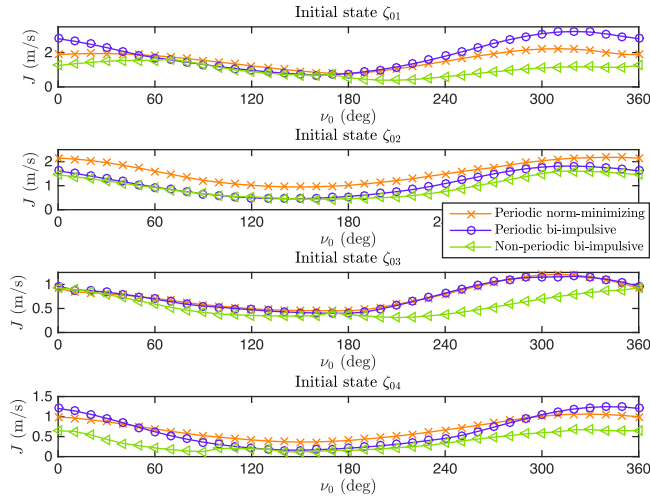

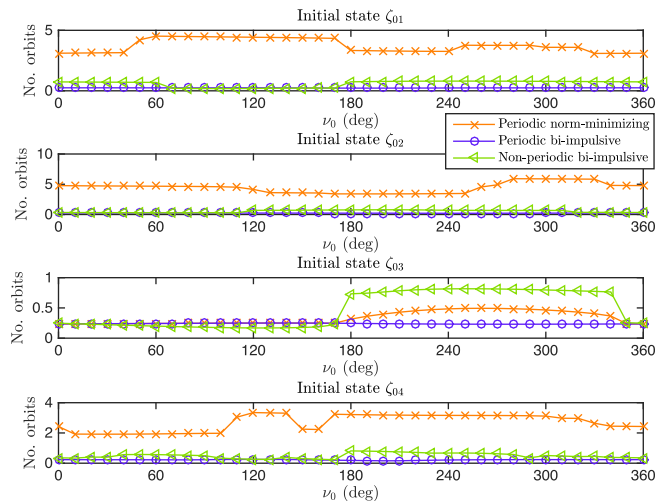Fig. 4: Comparison of the cost J among the three control laws for the initial states in (33).

Fig. 5: Comparison of the number of orbital periods ν_B among the three control laws for the initial states in (33).

All Figures 4, 5, 6, 7, 8 and 9 highlight that the speed of convergence to the bounding box $\mathcal{B}$ is relatively slow when using the first control law (of Section IV-A). In fact, from Table I, it is possible to observe that parameter ν_B is much larger for this control law than the one obtained in the two other cases. Figures 6, 7, 8 and 9 represent the trajectories of the follower satellite for an initial leader true anomaly of 180 (deg), and it can be seen that the trajectories corresponding to the first control law are much longer than the ones of the two other controls.

The periodic norm-minimizing control presents a slow convergence, while associated to an increased fuel consump-

ζ_0	Min. value	Periodic norm-minimizing	Periodic bi-impulsive	Non-periodic bi-impulsive
ζ_{01}	J	0.7722	0.6942	0.3942
	ν_B	3.0904	0.2230	0.1849
ζ_{02}	J	0.9448	0.4566	0.4402
	ν_B	3.4036	0.2013	0.2817
ζ_{03}	J	0.4522	0.3991	0.3108
	ν_B	0.2349	0.2306	0.1690
ζ_{04}	J	0.3634	0.1612	0.1187
	ν_B	1.9181	0.1592	0.2269

TABLE I: Minimum values of fuel consumption J (m/s) and angular time $\nu_{\mathcal{B}}$ for all the simulations presented in Figures 4 and 5.

tion. On the other hand, an advantage of this controller is that the solution evolves along periodic motions, thereby being fault tolerant. Instead, the two bi-impulsive solutions show a reduced fuel consumption with a strong preference for the non-periodic one, always leading to a more than substantial fuel saving.

Both the bi-impulsive control laws discussed in Sections IV-B and IV-C behave better than the previous one in terms of convergence speed. In fact the reference trajectory is tracked after the firing period $\bar{\nu}$ with zero error, by design.
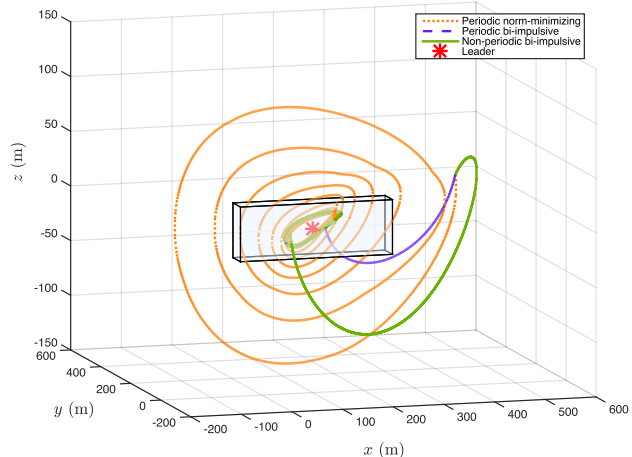

Fig. 6: Evolution of $\zeta_{1..3}$ with the three control laws from the initial state ζ_{01}.

VI. CONCLUSIONS

In this article, a new model, based on Floquet-Lyapunov theory, is developed in order to obtain a linear time-invariant free motion representation. The rendezvous problem is then recast as a stabilization problem for a periodic trajectory in a hybrid dynamical system framework. Two different control laws are developed and compared to a control scheme given in [5] which is re-interpreted in this hybrid context.

Alternative trade-offs should be investigated that adjust $\bar{\nu}$ within optimized fuel consumption under some constraint on the maximum distance reached during the transient.
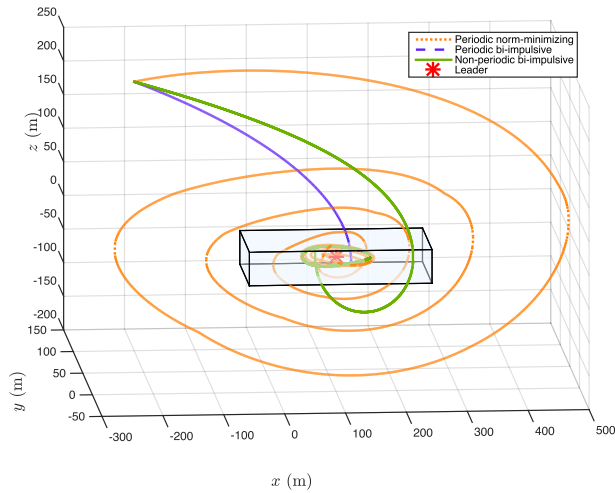
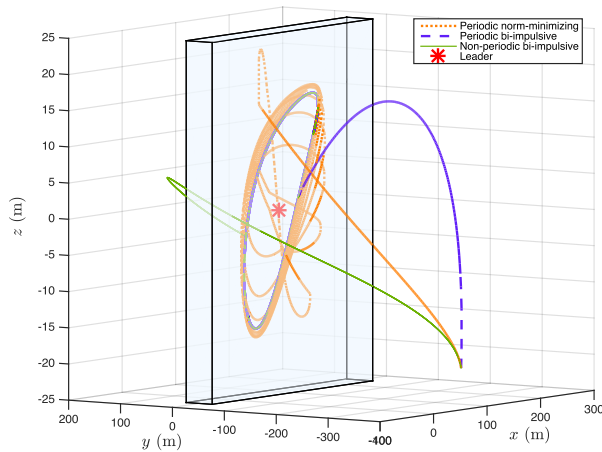Fig. 7: Evolution of $\zeta_{1..3}$ with the three control laws from the initial state ζ_{02}.

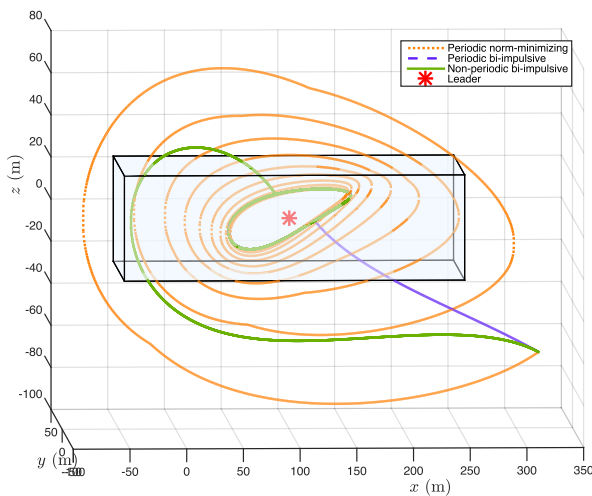Fig. 8: Evolution of $\zeta_{1..3}$ with the three control laws from the initial state ζ_{03}.

Fig. 9: Evolution of $\zeta_{1..3}$ with the three control laws from the initial state ζ_{04}.

The work presented in this paper is preliminary and a deeper study will be done regarding the bi-impulsive control methods. Formal proofs will also be provided in future works, such as the strict convexity property of the function appearing in Figure 3 that could lead to efficient convex optimization methods to evaluate control laws similar to the non-periodic bi-impulsive one appearing in this paper.

REFERENCES

[1] K.T. Alfriend and H. Schaub. Dynamics and control of spacecraft formations: Challenges and some solutions. *Journal of the Astronautical Sciences*, 48(2):249–267, 2000.
[2] A. Ben-Israel and T. NE Greville. *Generalized inverses: theory and applications*, volume 15. Springer Science & Business Media, 2003.
[3] G. Deaconu, C. Louembet, and A. Theron. Constrained periodic spacecraft relative motion using non-negative polynomials. In *American Control Conference (ACC), 2012*, pages 6715–6720, June 2012.
[4] G. Deaconu, C. Louembet, and A. Theron. Constrained periodic spacecraft relative motion using non-negative polynomials. In *American Control Conference (ACC), 2012*, pages 6715–6720, June 2012.
[5] G. Deaconu, C. Louembet, and A. Theron. A two-impulse method for stabilizing the spacecraft relative motion with respect to a periodic trajectory. In *Decision and Control (CDC), 2012 IEEE 51st Annual Conference on*, pages 6541–6546, Dec 2012.
[6] W. Fehse, editor. *Automated rendezvous and docking of spacecraft*. Cambridge Aerospace Series. Cambridge University Press, Cambridge, UK, 2003.
[7] R. Goebel, R.G. Sanfelice, and A.R. Teel. *Hybrid Dynamical Systems: modeling, stability, and robustness*. Princeton University Press, 2012.
[8] P. Gurfil. Relative motion between elliptic orbits: Generalized boundedness conditions and optimal formationkeeping. *Journal of Guidance, Control and Dynamics*, 28(4):761–767, July 2005.
[9] G. Inalhan, M. Tillerson, and J.P. How. Relative dynamics and control of spacecraft formations in eccentric orbits. *Journal of Guidance, Control and Dynamics*, 25(1):48–59, January-February 2002.
[10] C. Louembet, D. Arzelier, and G. Deaconu. Robust rendezvous planning under maneuver execution errors. *Journal of Guidance, Control, and Dynamics*, 2015.
[11] I.M. Ross. 6 space trajectory optimization and l 1-optimal control problems. *Elsevier Astrodynamics Series*, 1:155–VIII, 2007.
[12] H. Schaub and J.L. Junkins. *Analytical mechanics of space systems*. Education Series. AIAA, Reston, Virginia, USA, 2003.
[13] J. Tschauner. The elliptic orbit rendezvous. In *AIAA 4th Aerospace Sciences Meeting*, Los Angeles, Californie, USA, Juin 1966.